TMA-Based Beamforming For Next Generation Satellite Communication Applications

Gebrehiwet Gebrekrstos Lema, Ashok Bandi, Eva Lagunas, Bhavani Shankar Mysore R, Joel Grotz*
*Interdisciplinary Centre for Security, Reliability and Trust (SnT), University of Luxembourg, *SES S.A., Luxembourg*
*e-mails:{gebrehiwet.lema, ashok.bandi, eva.lagunas, bhavani.shankar}@uni.lu, joel.grotz@ses.com**

2024 IEEE International Conference on Communications Workshops (ICC Workshops) | 979-8-3503-0405-3/24/$31.00 ©2024 IEEE | DOI: 10.1109/ICCWORKSHOPS59551.2024.10615526

***Abstract*—Low-Earth Orbit (LEO) satellite mega-constellations have attracted significant interest for their global network coverage and reduced latency with respect to their geostationary counterparts. LEO satellites are typically equipped with advanced antenna architectures, which allow spot-beam steering to specific areas within the field of view. With the aim to minimize onboard complexity, this paper studies the beam synthesis and steering using Time Modulated Arrays (TMA). By analyzing the properties of the on-off switching and their impact on the resulting beam footprint, this paper establishes the relationship between the pulse activation characteristics and the steering angle of the corresponding users in a downlink satellite-to-Earth transmission. The corresponding Signal-to-Noise Plus Interference Ratio (SINR) is derived and analyzed for multi-beam patterns with different inter-beam separations. We compare the performance of TMA-based LEO downlink transmission with conventional beamforming techniques, confirming the promising performance of TMA with reduced complexity. Finally, the TMA response is evaluated for practical channel estimation imperfections, demonstrating the degree of tolerance depending on the beam shape.**

***Index Terms*—next-generation satellite communications, onboard processing, beamforming, TMA**

I. Introduction

For geographical conditions and economic reasons, global coverage is not easy with terrestrial networks (TN) alone. While remote areas, seas, and flying objects can be connected using non-TNs (NTNs), base station deployment everywhere is expensive. LEO satellites attracted the interest of researchers for global coverage while leveraging short delay, low signal attenuation, and low launching cost, [1]. However, LEO satellites have lower beam coverage and increasing the number of satellites imposes additional costs and risks. Sophisticated beamforming techniques at the expense of computational complexity don't adhere to the limited computing resources. Onboard Processing (OBP) realizes on-orbit computing which is one of the fundamental elements of global coverage. However, there is limited processing and transmission power, memory, and spectral resources onboard. In satellite communication, parabolic antennas were used for several years. Later on, the phased array antennas dominated in which the radiation features were adjusted without antenna physical movement; and costs were reduced. Recently, satellite industries such as SES, deployed digital beamformers with flexible connectivity, employing transparent payloads [2]. However, power consumption and complexity continued challenging. Using N element conventional phased arrays, L-stream fully analog BF receiver requires L RF-front ends and a linear BF network with $L \times N$ phase shifters, [3]. This is still simpler than digital beamforming. The complexity of BF increases with the array size on top of the size and weight costs. A few array elements can also be designed to generate multiple beams using, for example, Butler-matrix [4]. However, the BF network complexity made it impractical for LEO satellite systems. Recently, TMAs replaced the phase shifters of phased arrays with switching sequences while still enabling multi-beam. In TMA, switching pulses generate sidebands (SBs) which were treated as a drawback for decades [5]. However, by smartly engineering the SBs, TMAs have shown promising potential solutions for multi-beam satellite applications. Despite their BF network, TMAs have often intrinsic beam steering and interference among beams [6]. Though complexity can be promoted, the flexibility with the harmonic BF can be enhanced by TMA switching sequences, [7] and [8]. The optimal switching sequences and antenna positions were studied for 5G applications, [9]. A transceiver network is also proposed using TMA [10], however, the SINR impacts of the TMA structure and the beam steering should be studied especially in the satellite industry context. Inspired by its additional control parameter and directional beams, on its recent call for secure satellite communication, the European Space Agency (ESA) highlights TMA work [11]. The significance of TMA-based BF has been studied for satellite communication applications, [12]. The pattern synthesis of TM structure is studied [13]. Motivated by its simplified BF structure and single RF front end for multi-beam applications, this work focuses on TMA for satellite applications. Noticing its interference, performance, and steering are not studied for LEO satellite systems, this paper works to fill the challenges to realize TMA for next-generation satellite communication applications. The contributions of the paper are:

- The performance and complexity trade-off between TMA and the conventional array is evaluated.
- A recursive mathematical TMA switching sequences relationship is provided, which simplifies TMA BF design.
- To evaluate the effectiveness of the proposed structure, the beam steering and SINR are formulated & evaluated.
- TMA practicality of channel estimation error is evaluated.

This work has been supported by the Luxembourg National Research Fund (FNR) under the project INSTRUCT (IPBG19/14016225/INSTRUCT).

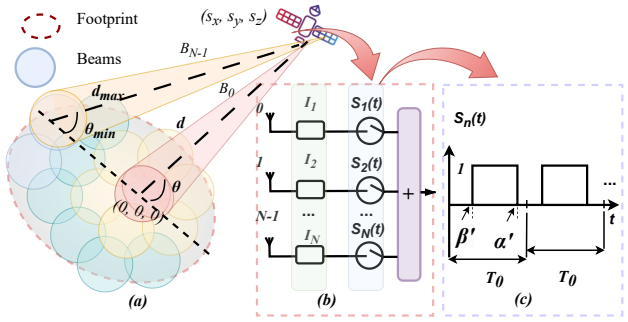

Fig. 1: (a) Beam layout, (b) TMA, and (c) switch control pulse

The rest of the paper is structured as: Section II discusses the system model of TMA in satellite. In Section III, beam steering and SINR are formulated. In Section IV, results are discussed and finally, Section V summarises the paper.

II. System Model

We consider a multi-beam satellite communication scenario as shown in Fig.1(a) wherein a LEO satellite communicates with User Terminals (UTs) each being equipped with a single receive antenna of gain G_r. Without loss of generality, each beam is assumed to serve one UT located at its centre in the downlink. To meet the demands, the system bandwidth is reused in the beams leading to co-channel interference. This interference is naturally determined by the beam pattern layouts, which, in turn, are governed by the array structure and its excitation. Hence, the SINR at the user is affected as a result of the array structure and beam pattern layouts. These will be studied in the sequel.

A. TMA radiation pattern design

In the proposed TMA antenna architecture, as shown in Fig. 1(b), the excitation phases of the n^{th} antenna element of the conventional Uniform Linear Array (ULA) are replaced by simple ON-OFF RF switches. $S_n(t)$ denotes the switching function of the n^{th} antenna element. A typical switching function, depicted in Fig. 1(c), is periodic with period T_0. The n^{th} antenna element is controlled by the n^{th} RF-switch, $S_n(t)$, and this can be expressed as:

$$S_n(t) = \begin{cases} 1, & \text{if } \beta'_n \leq t \leq \alpha'_n \\ 0, & \text{otherwise.} \end{cases} \tag{1}$$

where, $\beta'_n \geq 0$ and $\alpha'_n \leq T_0$ denote the switching ON and OFF instants of $S_n(t)$, respectively. The normalized switching delay and duration of the n^{th} pulse are, respectively, given by:

$$\beta_n = \beta'_n/T_0 \text{ and } \alpha_n = (\alpha'_n - \beta'_n)/T_0.$$

Suppose an LEO satellite is equipped with N-isotropic elements of a linear array. The far-field radiation pattern of an N-element TMA in the elevation θ and azimuth ϕ directions $AF(\theta, \phi)$, simplified as $AF(\theta, t)$ hereon, is given by:

$$AF\,(\theta, t) = \sum_{n=0}^{N-1} e^{j2\pi f_c t} S_n(t) I_n e^{jkz_n \cos(\theta)}, \tag{2}$$

where, $z_n = nd, \;\; n = 0, \; 1, \cdots, N-1$ and d is the inter-element spacing. $I_n = |A_n|e^{-j\phi_n}$ is the polar form of the complex static excitation current of the n^{th} antenna element. f_c is the carrier frequency, and k is the wave number ($k = \frac{2\pi}{\lambda}$) for a wavelength $\lambda = \frac{c}{f_c}$, and c is the speed of light. Since $S_n(t)$ is a periodic function, its Fourier series is:

$$S_n(t) = \sum_{q=-\infty}^{\infty} S'_{n,q} e^{jq2\pi F_0 t}, F_0 = 1/T_0 \tag{3}$$

where $S'_{n,q}$ is the Fourier coefficient of the q^{th} harmonic component. Substituting (3) in (2), $AF(\theta, t)$ is expanded as:

$$AF(\theta, t) = \sum_{q=-\infty}^{\infty} \sum_{n=0}^{N-1} S'_{n,q} I_n e^{jkz_n \cos(\theta)} e^{j2\pi t(f_c + qF_0)}. \tag{4}$$

Using Fourier theory, we obtain $S'_{n,q}$ as:

$$\begin{aligned} S'_{n,q} &= \frac{1}{T_0} \int_{\beta'}^{\alpha'} S_n(t) e^{-jq2\pi F_0 t} dt, \in \mathbb{R} \\ &= \alpha_n \,\mathrm{sinc}(\pi q \alpha_n) e^{-j\pi q(2\beta_n + \alpha_n)}. \end{aligned} \tag{5}$$

As the higher-order harmonics generate little radiation, we confine the Fourier series harmonics to $-\,Q \leq q \leq \;Q$. With this assumption and by substituting (5) into (4), the complete TMA AF expression is given by:

$$\begin{aligned} AF(\theta, t) = \sum_{q=-Q}^{Q} \sum_{n=0}^{N-1} I_n \alpha_n \,\mathrm{sinc}(\pi q \alpha_n) e^{-j\pi q(\alpha_n + 2\beta_n)} \\ \times e^{jkz_n \cos(\theta)} e^{j2\pi(f_c + qF_0)t}, \end{aligned} \tag{6}$$

and from equation (6), we can observe that the far-field pattern can be controlled by the delay and the duration of the TMA switching parameters, β_n and α_n. Hence, TMA can replace the expensive phase shifters used in phased array systems.

B. Downlink signal model

We consider the TMA-based multi-beam architecture as shown in Fig. 2. The i^{th} user beamforming vector over the q^{th} harmonic component is expressed as $\mathbf{w_i} = [w_{-Q,i}, \cdots, w_{Q,i}]^T, i = 1, ..., L$. Assuming we have L users to transmit for, the signal available for the i^{th} user is:

$$b_i(t) = \sqrt{p_i}\tilde{b}_i(t), \tag{7}$$

where $\tilde{b}_i(t)$, p_i, and $b_i(t)$ are the baseband signal, transmit power, and assigned power baseband signal of user i, respectively. The downlink signal model splits into three phases:
(1) User signals mapping to beams: In this step, the baseband

signal available for the i^{th} user mapped to the q^{th} harmonic component is $c_{q_i}(t)$:

$$c_{q_i}(t) = e^{j2\pi q_i F_0 t} w_i b_i(t). \tag{8}$$

(2) Digital to analog conversion: We have L signals, $\{c_{q_i}(t)\}_{i=1}^{L}$, to be transmitted to L users. The modulated signals are combined into single-channel analog signals, defined as:

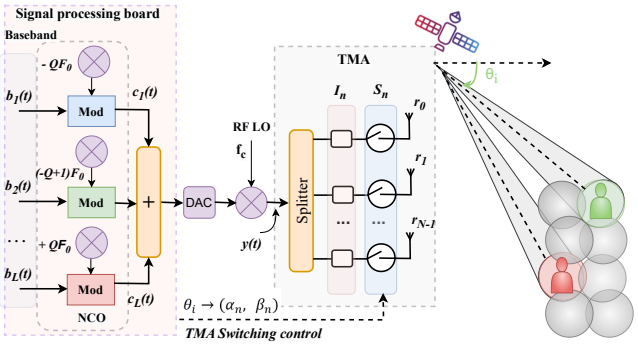

Fig. 2: Detailed TMA beamforming structure

$$y(t) = \sum_{i=1}^{L} \sum_{q_i=-Q}^{Q} w_i b_i(t) e^{j2\pi(f_c + q_i F_0)t}. \tag{9}$$

(3) TMA analog beamforming: The analogue signal $y(t)$ is fed to the TMA system using a power splitter to excite the different antenna elements. Finally, by applying the same Fourier decomposition at the TMA switching, the modulated signal at the n^{th} array element is expressed as:

$$r_n(t) = \frac{1}{\sqrt{N}} \left[\sum_{\bar{q}_i=-\infty}^{\infty} S'_{n,\bar{q}_i} e^{j2\pi \bar{q}_i F_0 t} \right] y(t) e^{jkz_n \cos(\theta_i)} \tag{10}$$

the term $\frac{1}{\sqrt{N}}$ is introduced to indicate the normalized transmit power splits among the N elements. For the harmonic order q_i, a new harmonic component is introduced at the TMA switching with harmonic order $\bar{q}_i$, $\bar{q}_i = -q_i$ and $(S'_{n,\bar{q}_i})^* = S'_{n,-q_i}$. The index of the user that belongs to q_i is systematically transferred to the $-q_i$ index so that the carrier frequency of all users is fixed at f_c. The harmonic components align with the direction of departure (DOD). Then, at the n^{th} antenna element, the radiated signal $r_n(t)$ is given by:

$$r_n(t) = \frac{1}{\sqrt{N}} e^{j2\pi f_c t} \sum_{q_i=-Q}^{Q} S'_{n,-q_i} \sum_{i=1}^{L} w_i b_i(t) e^{jkz_n \cos(\theta_i)} \tag{11}$$

For each user i, the received signal at the carrier frequency f_c is filtered, down-converted, and sampled to the corresponding baseband signal. The sampled baseband signal of the i^{th} user, z_i, over the channel $h_{i,n}$ is: $z_i(t) = h_{i,n} r_n(t)$. At the receiving end, the sampled baseband signal is

$$z_i(t) = \frac{1}{\sqrt{N}} \sum_{n=0}^{N-1} h_{i,n} \sum_{q_i=-Q}^{Q} S'_{n,-q_i} w_i b_i(t) e^{jkz_n \cos(\theta_i)}, \tag{12}$$

and assuming the channels are reciprocal, this along with a noise $n(t)$ can be represented in a compact form as:

$$z_i(t) = 1/\sqrt{N}[\mathbf{H}^T \mathbf{S'}^H \mathbf{W} \mathbf{b}(t) \phi] + \mathbf{n}(t). \tag{13}$$

Where,

$$\mathbf{z}_i(t) = [z_1(t), \cdots, z_L(t)]^T$$
$$\mathbf{n}(t) = [n_1(t), \cdots, n_L(t)]^T$$
$$\mathbf{b}(t) = [\sqrt{p_1} b_1(t), \cdots, \sqrt{p_L} b_L(t)]^T$$
$$\mathbf{w} = [w_1, \cdots, w_L]$$
$$\mathbf{H}^T = [\mathbf{h_1}, \cdots, \mathbf{h_L}]^H$$
$$\boldsymbol{\phi_i} = [\boldsymbol{\varphi}_{\theta_1}, \cdots, \boldsymbol{\varphi}_{\theta_L}], \boldsymbol{\varphi}_{\theta_i} = [1, \cdots, e^{jkz_{N-1}cos(\theta_i)}]^T$$

$$\mathbf{S'} = \begin{bmatrix} a_{0,-Q} & a_{1,-Q} & \cdots & a_{N-1,-Q} \\ a_{0,-Q+1} & a_{1,-Q+1} & \cdots & a_{N-1,-Q+1} \\ \vdots & \vdots & \ddots & \vdots \\ a_{0,Q} & a_{1,Q} & \cdots & a_{N-1,Q} \end{bmatrix}$$

Finally, we can apply the Zero Forcing (ZF) detector on the received signal given in (13). The ZF detector enables us to suppress interference coming from other users and this can be done using the pseudo-inversion of the combination of the channel ($\frac{1}{\sqrt{N}} \mathbf{H}^T \mathbf{S'}^H$). We can design the pseudo-inversion beamforming matrix $\mathbf{W_{ZF}}$ as:

$$\mathbf{W}_{ZF} = c_{ZF} (\mathbf{H}^T \mathbf{S'}^H)^{\dagger} \tag{14}$$

where, $(.)^{\dagger}$ implies the pseudo inversion,

$$c_{ZF} = \sqrt{P / tr(\mathbf{H^T S'^H S' H^*})},$$

and c_{ZF} is the power normalization factor, P is the total transmitted power, and tr(·) is the trace of a matrix. Using the ZF matrix $\mathbf{W}_{ZF}$, we can multiply (13) to distinguish the desired signal. Where, $[.]^{\mathbf{T}}$ is transpose and $[.]^{\mathbf{H}}$ is Hermitian.

III. Problem Formulation

A. DOD to TMA switching parameters mapping

The users' DOD to the TMA switching parameters (α_n, β_n) mapping updates for each user to swiftly radiate the individual user signal to the desired position. The DOD to the TMA switching parameters mapping has a two-fold objective : (1) map the users' DOD to the TMA switching parameters to steer the main lobe and (2) assess the impact of pattern sidelobes through SINR. The first objective maps θ_i to α_n and β_n without major radiation pattern defects. The second objective evaluates the impact of the proposed scheme on SINR. We first detail the nature of the relationship among θ_i, α_n, and β_n. Without loss of generality, assuming I_n is unity, we rewrite the TMA pattern as,

$$AF_{q_i} = \sum_{n=0}^{N-1} C_n^{q_i} e^{j\{-\pi q_i(\alpha_n + 2\beta_n) + kz_n \cos(\theta_i)\}} e^{j2\pi(f_c + q_i F_0)t}, \tag{15a}$$

$$C_n^{q_i} = \frac{\sin(\pi q_i \alpha_n)}{\pi q_i}, \tag{15b}$$

where we have used $\mathrm{sinc}(x) = \sin(x)/x$. From AF_{q_i} shown in (15a), the phase part is responsible for the steering control. This ensures that the maximum direction of a beam aligns with the corresponding user location. For a small value of ϑ, the trigonometric function $\mathrm{sinc}(\vartheta)$ tends to unity. Therefore, for every array element n and every harmonic order q_i, the excitation weight given in (15b) can be written as,

$$C_n^{q_i} = I_n \alpha_n \,\mathrm{sinc}(\pi q_i \alpha_n) \approx \alpha_n.$$

This is realistic because the switching parameters are practically very small. Of course, the oscillatory behaviour of the trigonometric function emerges at higher harmonic orders. The beam steering at the desired angle θ_i, served by the q_i^{th} harmonic order is calculated from the phase of $AF_q(\theta, t)$:

$$j[kz_n \cos\theta_i - \pi q_i(\alpha_n + 2\beta_n)] = 0. \tag{16}$$

This results in all the terms adding in phase, increasing the gain. Then, the relationship between θ_i, α_n, and β_n is:

$$\alpha_n + 2\beta_n = \frac{nkd}{\pi q_i}\cos\theta_i, n = 0, 1, ..., N-1 \tag{17}$$

To reasonably formulate the user position θ_i to TMA switching parameters mapping, we briefly go through how the TMA switching parameters control the TMA radiation pattern. For this purpose, we have described (17) as follows:

$$\begin{aligned}
&\text{Let } \frac{nkd}{\pi q_i}\cos\theta_i = nc_i,\\
&\text{where } c_i \text{ depends on the } i^{th} \text{ user location, } \theta_i\\
&\text{Note that the } i^{th} \text{ user is served by the } q_i^{th} \text{ beam,}\\
&\text{Then, } \alpha_n + 2\beta_n = nc_i,\\
&\alpha_{n+1} + 2\beta_{n+1} = \alpha_n + 2\beta_n + c_i,\\
&\alpha_{n+2} + 2\beta_{n+2} = \alpha_{n+1} + 2\beta_{n+1} + c_i,\\
&\quad\vdots \qquad\quad \vdots \qquad\quad \vdots \qquad\quad \vdots\\
&\alpha_N + 2\beta_N = \alpha_{N-1} + 2\beta_{N-1} + c_i.
\end{aligned} \tag{18}$$

The expression given in (18), mathematically formulated for the first time in this work, indicates that the successive values of $\{\alpha_n\}_n$ and $\{\beta_n\}_n$ are recursive. This allows us to simplify and trace computational complexity to determine α_n and β_n. This gains significant simplicity in finding the optimal switching sequence solution over time-consuming meta-heuristic algorithms or try-and-error methods. It should be noted that many researchers apply meta-heuristic algorithms, [14], to determine the TMA switching sequences which neither guarantee the optimal solution nor computing resources economical.

1) Assumptions and considerations: In this paper, we assume that each element is ON for $(1/N)^{th}$ fraction of the period throughout the paper unless specified. We consider that the 'time delay' β_n progressively increases as n/N only when we refer to beam shapes that are without beam steering.

2) Beam steering using TMA structure: This progressive delay β_n is used to realize the electronic beam steering in the proposed TMA structure. For the beam steering case, β_n takes (19). Since we fix α_n, then the value of α_n together with (15b) and (17), for every harmonics q_i and every switching sequence n, we can see the novelty to determine the beam steering by calculating the delay $\beta_n^{q_i}$ as follows:

$$\beta_n^{q_i} = \frac{1}{2\pi q_i}[nkd\cos\theta_i - \sin^{-1}(\pi q_i |C_n^{q_i}|)]. \tag{19}$$

For a general case, (19) concludes the beam steering capability. The harmonic beams can be directed to any desired direction by merely using the switching parameters. For example, for half wavelength inter-element spacing, for the first harmonic component, (19) can be written as

$$\beta_n^1 = \frac{1}{2}[n\cos\theta_1 - \sin^{-1}(\pi |C_n^1|)] \tag{20}$$

For the normalized case, the excitation weight has to vary within the range $[0, 1]$. Therefore, $\sin(\pi\alpha_n)$ cannot be negative and varies in $[0, 1]$. Hence, α_n varies in the range $[0, 0.5]$.

B. Impact of TMA Structure on SINR

In TMA, the main signal power of the i^{th} user, received from the q_i^{th} harmonic component is represented by $|h_i AF_{q_i}(\theta_i, t)|^2 p_i$. As described in the TMA pattern design, the $AF_{q_i}(\theta_i, t)$ is composed of S'_{n,q_i} and hence the switching parameters. However, as seen from the equation (13), it follows that multiple users' signals are transmitted on the same carrier frequency leading to interference. The interfering power coming from all of the other users on q_j and channel h_j can be defined as $\sum_{j=1, j\neq i}^{L-1} |h_j AF_{q_j}(\theta_j, t)|^2 p_j$. The SINR received for the i^{th} user can be summarized as:

$$\begin{aligned}
SINR_{q_i} &= \frac{|h_i AF_{q_i}(\theta_i, t)|^2 p_i}{B\sigma_n^{q_i} + \sum_{j=1, j\neq i}^{j=L} |h_j AF_{q_j}(\theta_i, t)|^2 p_j},\\
\text{here, } |AF_{q_k}(\theta_k, t)|^2 &= \sum_{n=0}^{N-1} |I_n S'_{n,q_k} e^{jkz_n\cos(\theta_k)}|^2,\\
|S'_{n,q_k}|^2 &= |\alpha_n|^2 |\mathrm{sinc}^2(\pi q_k \alpha_n)|, q_j \neq q_i,
\end{aligned} \tag{21}$$

where $q_k = q_i$ for the desired signal and $q_k = q_j$ for the interfering signal, $\sigma_n^{q_i}$ is the ${q_i}^{th}$ Additive White Gaussian Noise (AWGN) with zero mean and constant variance.

From equation (21), the SINR largely depends on the following three parameters: (i) the sidelobe level of the TMA radiation pattern, (ii) the beamwidth, and (iii) the angular separation between the beams. To address this challenge, while the first two depend on the TMA pattern, the third indicates resource management. Additionally, because the $AF(\theta, t)$ depends on the switching parameters, number of elements, static excitation weight and phase of the array elements, the SINR again depends on all of these parameters. The TMA switching parameters largely determine the radiation pattern and hence the interference. On top of the switching-based pattern control, we have introduced a tapering technique to

reduce the SLL and the SINR performance. For the i^{th} user with a desired target SLL R, the tapering technique enables us to design the excitation weights of the AF. The tapering details are given in [15] for an even number of elements N. Considering the complexity and performance, the multi-beam TMA, SLL, beamwidth, and spacing impacts are evaluated.

Assuming the TMA is capable of generating multiple beams, we have evaluated the SINR by setting a scenario where we have B_N beams serving UTs downlink, $B_0, \cdots, B_{N-1}$, as shown in Fig. 1(a). The transmit power and Effective Isotropic Radiated Power (EIRP) of the B_n^{th} beam containing the desired signal are $\tilde{p}^d_{B_n}$ and $\tilde{p}^d_{B_n} G^d(\theta, \phi)$, respectively. Here, $G^d(\theta, \phi)$ is the gain of the beam with the desired signal in the elevation (θ) and azimuth (ϕ), equivalent to $|AF(\theta, \phi)|^2$. Then, the received power of the desired signal, $p^d_{B_n}$, is given by $[\tilde{p}^d_{B_n} G^d(\theta, \phi) G_r(\theta, \phi)]/\Gamma$, where, $G_r(\theta, \phi)$ is the gain of the UT and the Γ indicates the losses, that are free space loss, atmospheric loss, rain loss, polarization loss, and antenna misalignment loss. Similarly, the received power of the interfering beam, $p^i_{B_m}$, is given by: $[\tilde{p}^i_{B_m} G^i(\theta, \phi) G_r(\theta, \phi)]/\Gamma$, where, $\tilde{p}^i_{B_m}$ is the transmit power of the interfering beam $B_m, m \neq n$ and $G^i(\theta, \phi)$ is the gain of the interfering beam towards the UT position.

At each beam, the SINR of a user is summarized as,

$$SINR_{B_n} = \frac{p^d_{B_n}}{KTB + \sum_{m=1}^{B_N} p^i_{B_m}} \tag{22}$$

where, K, T, B are the Boltzmann constant, system temperature, and noise bandwidth, respectively. While (21) enables us to study the SINR impact of the proposed structure, (22) enables us to focus on the inter-beam SINR.

IV. Numerical Results

In this paper, we consider the LEO satellite system given by 3GPP Rel.16 technical specification of NR that supports NTN, shown in Table I. We assume the LEO satellite transmits to a handheld user, located at the centre of the beam. The coverage and beam shapes, shown in Fig. 1(a), are based on [16]. To evaluate the effectiveness of the proposed beamforming structure, the multi-beam patterns, gain, and complexity are studied based on Table I.

TABLE I: Evaluation parameters

Parameter	Symbol	Setting
Orbital height	H	600 km
$3dB$ beamwidth	Ω	4.4°
Carrier frequency	f_c	2 GHz
Receiver gain	G_r	0 dB
Noise bandwidth	B	30 MHz
Reference Temperature	T	290 k
Boltzmann's constant	K	$1.23x10^{-23}$
Satellite EIRP	E_r	34 dBW/MHz

First, to compare the complexity and gain of ULA and TMA, we have used the number of elements, beamforming networks, normalized gain, and beamwidth parameters. An efficient typical N element ULA-based Butler Matrix generates N beams. This is realized using $N \times N$ matrix networks, N phase shifters, $2N$ crossovers, and more than N quadrature hybrid, [17]. In a general case, as indicated above, an N element ULA with L stream fully analog beamforming requires L RF-front ends and $L \times N$ phase shifters. The ULA digital beamformers are even more costly because of the number of RF chains per antenna element. On the other hand, the proposed TMA supports multiple users with a single RF front-end using a time-switching function. To evaluate the

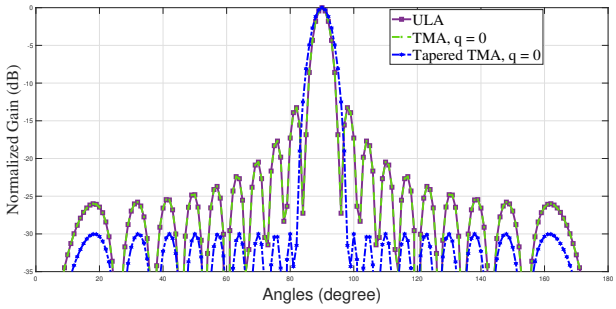

(a) Gain of ULA, TMA, and Tapered TMA

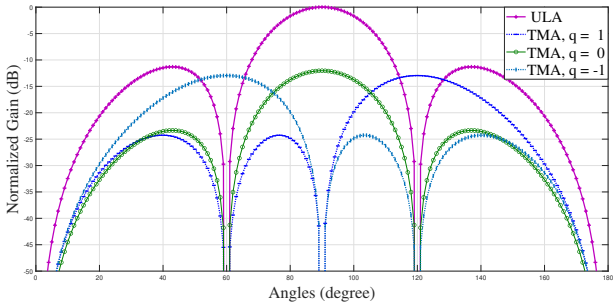

(b) Gain of ULA and TMAs

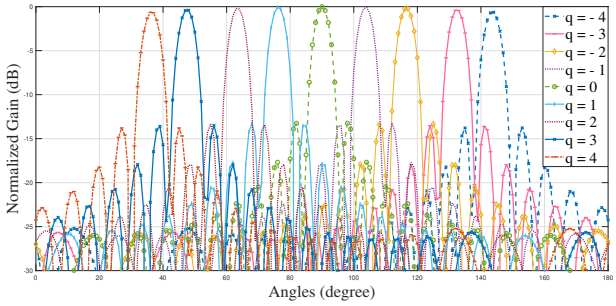

(c) TMA for multi-beam

Fig. 3: Summary of beam shapes and capabilities using ULA and TMA beamforming structures

TMA performance, we study three cases:
(i) Single beam case: To evaluate the gain and complexity of ULA and TMA, their radiation pattern is simulated for the same number of elements, $N = 20$, as shown in Fig. 3(a). A TMA with full period α_n, at $q = 0$, ULA and TMA have the same gain. The Tapered TMA is also included

to evaluate the beam shape. In Fig. 3(a), the Tapered TMA enables high gain at the expense of beamwidth. The Tapered TMA has already a high gain, however, to compensate for the increased beamwidth, the number of elements must increase which increases complexity.
(ii) Three-beam case: As shown in Fig. 3(b), three TMA beams are generated using fewer number of elements. The three TMA beams and ULA beam have the same beamwidth but the ULA outperforms in gain. However, ULA needs more number of elements or a complex BF network to generate three beams as TMA does.
(iii) Nine-beam case: using the same number of elements and the same RF front-end, nine beams are generated simultaneously using TMA as shown in Fig. 3(c). To generate 9 beams, TMA doesn't need further procedures. For the ULA, to generate the same number of 9 beams as TMA and the same beam characteristics, we need a large number of elements or a very complex beamforming network. The remaining cost depends on the beamforming network of ULA. With ULA, we can achieve the multi-beam with multiple RF chains while a single RF chain is enough in TMA. Therefore, due to the complexity, size, and weight, the ULA-based beamforming structure becomes challenging to apply in the limited computing resources associated with LEO satellite OBP systems.

A. *Beam direction control using TMA switching parameters*

In TMA, the direction of the main lobe is a function of the TMA switching parameters. As the maximum gain is achieved when the main beam is directed to the user position, the electronic beam control determines both the interference and gain. The beam steering also enables beam flexibility in resource management. The ground beams and polar plot shown in Fig. 4 verified that a beam has been directed over 260 kilometers from its initial position towards a newly assigned user position of $\theta_i = 60°$. As the onboard control unit steers the beam in the time domain, beam squinting is no longer a challenge.

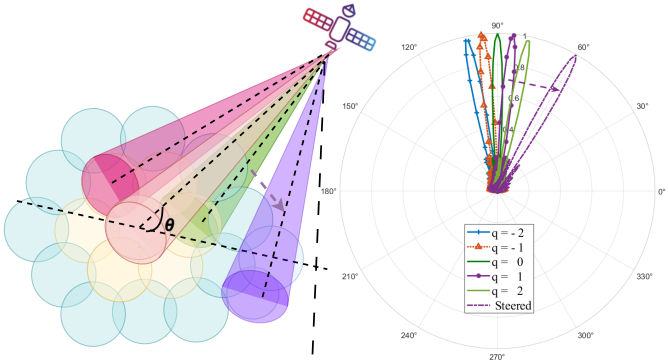

Fig. 4: Beam steering using TMA switching parameters

B. *SINR analysis*

To evaluate the performance of the proposed structure, a multi-beam LEO satellite is assumed located at the Earth-centred-Earth-fixed reference (ECEF) of $6,978,140$ km and its latitude and longitude are located in central Europe, $49.8°N, 6.13°E$. We consider a seven-beam scenario where a handheld receiver is located at the center of the central beam and the rest six beams uniformly encircle the central beam in 2D as shown in Figures 1(a) and 4. The six beams interfere with the user served by the central beam. Since we have shown the gain difference and SINR-gain dependency in Section III B, in this subsection we focus on beamwidth (Ω). we assume the satellite is equipped with TMA and Tapered TMA. First, in line with 3GPP Rel.16 technical specification, we consider $4.4°$ beamwidth. From Fig. 5, we can observe that the Tapered TMA performs a little better SINR because of its superior gain. However, the Tapered TMA increases the SINR performance at some array size cost. Then, we have increased the beamwidth to $7.0°$. The $2.6°$ beamwidth increase results in an average of 10 dB SINR loss. Hence, both the gain and beam shape largely impact SINR. Additionally, we can observe that SINR increases with increasing inter-beam spacing. However, after a certain level, the SINR doesn't increase because of the noise limit. In general, the array structure and size determine not only the weight and cost of the satellites but also the system SINR.

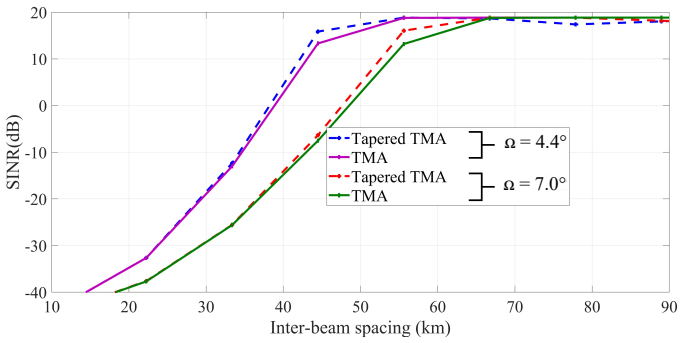

Fig. 5: SINR impacts of TMA and Tapered TMA

To further describe the coverage and potential interference, we generate 37 beams based on the 3GPP.811 requirements. By considering the adjacent beam spacing and the ground beam distribution of the TN, 3GPP recommended a 37-beam layout on 3 distinct "tiers". The LEO satellite is located at the ECEF,

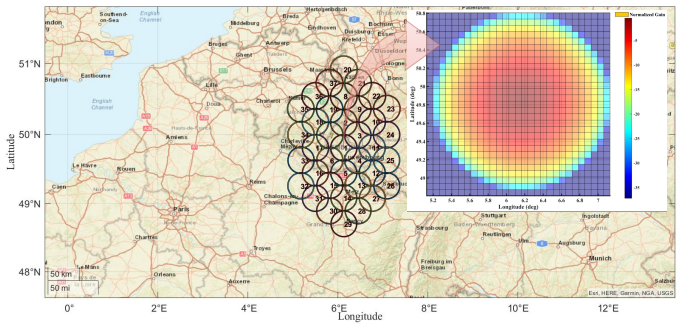

Fig. 6: Geographic beam pattern layout

as specified above. The $90°$-bore-sight of the centre of the beam is set Luxembourg, $49.8153° N, 6.1296° E$. The coverage of the 37-beam layout and the normalized gain distribution of the central beam is shown in Fig. 6.

By employing the multi-beam steering given in (19), each beam can be independently steered using the TMA switching parameters. Similarly, the TMA array size and switching parameters enable beam-shaping. The spatial reuse of the frequency increases system capacity. From Fig. 6, we can observe that by adapting the beamwidth we can increase the coverage of the beams. However, as the number of frequency reuse per area is reduced, the system capacity decreases. Besides, larger geographic area coverage more likely overlaps with adjacent beams which again reduces capacity.

C. Channel estimation analysis

To evaluate the TMA array response practicality in imperfect channel estimation, the first harmonic component is used to receive a user signal under Additive White Gaussian Noise channel. We assume the incoming signal is modulated by Binary Phase Shift Keying (BPSK) and the proposed TMA setup is used to receive the signal. We studied perfect and imperfect beam alignment in the Direction of Arrival (DoA) cases. In the perfect alignment case, the signal is collected using the maximum response of the TMA beam and in the imperfect alignment case, the array response points $2°$ misalignment. Finally, $100,000$ bits are transmitted and the Bit Error Rate (BER) is evaluated for a range of signal-to-noise ratios (SNR) as shown in Fig. 7. The same evaluation is

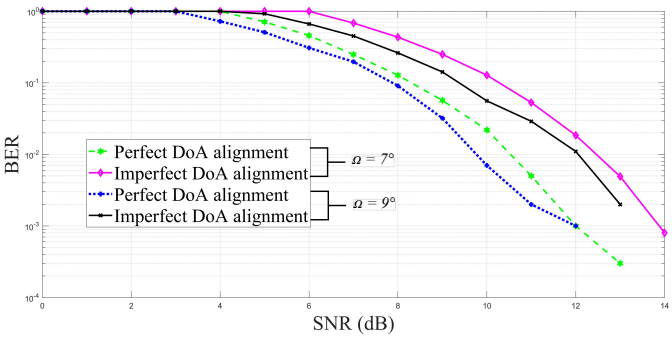

Fig. 7: Channel estimation response

repeated for a different beamwidth as shown in Fig. 7. In both beamwidth cases, the perfect alignment slightly outperforms the misaligned ones, giving room for practical imperfections and this depends on the operating beamwidth.

V. CONCLUSION

In this work, we highlighted the OBP solutions and challenges for global coverage. The multi-beam synthesis, beam steering, and SINR are formulated to evaluate the performance of the proposed BF architecture. The complexity and performance of ULA and TMA structures are compared. In the multi-beam case, TMA has shown promising simplicity at the expense of gain. The numerical results enabled us to analyze the complexity, beam shape, beam steering, and SINR impacts of the proposed structure. Finally, the channel estimation practicality is evaluated using the TMA harmonic component response. In future work, we will further focus on TMA switching designs and SINR-enhancing strategies.

REFERENCES

[1] X. Wang, N. Deng, and H. Wei, "Coverage and Rate Analysis of LEO Satellite-to-Airplane Communication Networks in Terahertz Band," *IEEE Trans. Wireless Commun*, vol. 22, no. 12, pp. 9076–9090, 2023.

[2] P. J. Honnaiah, E. Lagunas, S. Chatzinotas, and J. Krause, "Demand-Driven Beam Densification in Multibeam Satellite Communication Systems," *IEEE Transactions on Aerospace and Electronic Systems*, vol. 59, no. 5, pp. 6534–6554, 2023.

[3] S.-M. Moon, S. Yun, I.-B. Yom, and H. L. Lee, "Phased Array Shaped-Beam Satellite Antenna With Boosted-Beam Control," *IEEE Trans. Antennas Propag*, vol. 67, no. 12, pp. 7633–7636, 2019.

[4] A. K. Pandey, "Phased Array Antenna with Beamforming Network for 5G mmWave Communication System," in *2020 50th European Microwave Conference (EuMC)*, 2021, pp. 364–367.

[5] Q. Zeng, P. Yang, L. Yin, H. Lin, C. Wu, F. Yang, and S. Yang, "Phase Modulation Technique for Harmonic Beamforming in Time-Modulated Arrays," *IEEE Trans. Antennas Propag*, vol. 70, no. 3, pp. 1976–1988, 2022.

[6] Z. Li, F. Yang, Y. Chen, S.-W. Qu, J. Hu, and S. Yang, "Wideband Receive Beamforming Based on 4-D Antenna Arrays With Postmodulation," *IEEE Antennas Wirel. Propag. Lett.*, vol. 21, no. 4, pp. 740–744, 2022.

[7] Y.-Q. Yang, H. Wang, and Y.-X. Guo, "A Time-Modulated Array With Digitally Preprocessed Rectangular Pulses for Wireless Power Transmission," *IEEE Trans. Antennas Propag*, vol. 68, no. 4, pp. 3283–3288, 2020.

[8] G. Bogdan, K. Godziszewski, Y. Yashchyshyn, C. H. Kim, and S.-B. Hyun, "Time-Modulated Antenna Array for Real-Time Adaptation in Wideband Wireless Systems—Part I: Design and Characterization," *IEEE Trans. Antennas Propag*, vol. 68, no. 10, pp. 6964–6972, 2020.

[9] G. Maldonado, A. R. Maldonado, L. I. Balderas, and M. A. Panduro, "Time-Modulated Antenna Arrays for Ultra-Wideband 5G Applications, journal = Micromachines," vol. 13, no. 12, 2022.

[10] G. Ni, C. He, and R. Jin, "Harmonic-Based MIMO Transceiver With Time-Modulated Arrays," *IEEE Trans. Antennas Propag*, vol. 71, no. 9, pp. 7553–7565, 2023.

[11] J. Guo, L. Poli, M. A. Hannan, P. Rocca, S. Yang, and A. Massa, "Time-Modulated Arrays for Physical Layer Secure Communications: Optimization-Based Synthesis and Experimental Assessment," *IEEE Trans. Antennas Propag*, vol. 66, no. 12, pp. 6939–6949, 2018.

[12] C. He, Q. Chen, A. Cao, J. Chen, and R. Jin, "Application of the Time Modulated Array in Satellite Communications," *IEEE Wireless Communications*, vol. 26, no. 2, pp. 24–30, 2019.

[13] I. Kanbaz, G. O. Arican, Z. Noamadeh, and E. Aksoy, "An Optimization Approach to Synthesis of the Isoflux Pattern for GEO/MEO Satellites using Time Modulated Antenna Arrays," in *2022 30th Signal Processing and Communications Applications Conference (SIU)*, 2022, pp. 1–4.

[14] S.-R. Zhang, Y.-X. Zhang, and C.-Y. Cui, "Efficient Multiobjective Optimization of Time-Modulated Array Using a Hybrid Particle Swarm Algorithm With Convex Programming," *IEEE AWP Letters*, vol. 19, no. 11, pp. 1842–1846, 2020.

[15] A. Safaai-Jazi, "A new formulation for the design of Chebyshev arrays," *IEEE Trans. Antennas Propag*, vol. 42, no. 3, pp. 439–443, 1994.

[16] I. Leyva-Mayorga, B. Soret, M. Röper, D. Wübben, B. Matthiesen, A. Dekorsy, and P. Popovski, "LEO Small-Satellite Constellations for 5G and Beyond-5G Communications," *IEEE Access*, vol. 8, pp. 184 955–184 964, 2020.

[17] Y. Yamada, C. Z. Jing, N. H. Abd Rahman, K. Kamardin, I. I. Idrus, M. Rehan, T. Abd Latef, T. Abd Rahman, and N. Q. Dinh, "Unequally Element Spacing Array Antenna with Butler Matrix Feed for 5G Base Station," in *International Conference on TAFGEN*, 2018, pp. 72–76.